AIP | Journal of Renewable and Sustainable Energy

Mesoporous coupled ZnO/TiO2 photocatalyst nanocomposites for hydrogen generation

Abdulmenan M. Hussein, Luther Mahoney, Rui Peng, Harrison Kibombo, Chia-Ming Wu, Ranjit T. Koodali, and Rajesh Shende

Citation: Journal of Renewable and Sustainable Energy **5**, 033118 (2013); doi: 10.1063/1.4808263
View online: http://dx.doi.org/10.1063/1.4808263
View Table of Contents: http://scitation.aip.org/content/aip/journal/jrse/5/3?ver=pdfcov
Published by the AIP Publishing

Mesoporous coupled ZnO/TiO_2 photocatalyst nanocomposites for hydrogen generation

Abdulmenan M. Hussein,[1] Luther Mahoney,[2] Rui Peng,[2] Harrison Kibombo,[2] Chia-Ming Wu,[2] Ranjit T. Koodali,[2] and Rajesh Shende[1,a)]
[1]*Department of Chemical and Biological Engineering, South Dakota School of Mines & Technology, Rapid City, South Dakota 57701-3901, USA*
[2]*Department of Chemistry, University of South Dakota, Vermillion, South Dakota 57069, USA*

(Received 19 March 2013; accepted 17 May 2013; published online 4 June 2013)

The present work investigates mesoporous coupled ZnO-TiO_2 based nanocomposites towards photocatalytic hydrogen generation. The effect of Zn^{2+} loadings was examined on the photocatalytic activities of the sol-gel derived ZnO-TiO_2 nanocomposites employing a structure-directing template. ZnO-TiO_2 nanocomposites were characterized by powder X-ray diffraction, transmission electron microscopy, UV-vis diffuse reflectance spectroscopy, nitrogen isotherm, Raman, and electrochemical impedance spectroscopy (EIS) methods. The photocatalytic H_2 evolution of the ZnO-TiO_2 suspensions was evaluated in an aqueous methanol medium under UV illumination. The Zn^{2+} concentrations utilized to prepare ZnO-TiO_2 nanocomposites were found to have significant effect on the specific surface area, pore volume, and photocatalytic activity. The H_2 evolution results obtained with ZnO-TiO_2 nanocomposites were compared with H_2 generation using commercial TiO_2 P25 and individual ZnO nanoparticles. The photocatalytic activity of ZnO-TiO_2 composite enhanced significantly as compared to P25 or ZnO nanoparticles. With respect to an increment in Zn^{2+} loading, the photocatalytic activity of the composite increased and reaching an optimal H_2 production of 17.3 ml/g of catalyst for the ZnO-TiO_2 composite containing 30 wt. % ZnO (30ZnO). The specific surface area of the samples increased from 19 (single ZnO) to 122 m^2/g for ZnO-TiO_2 composite containing 50 wt. % ZnO (50ZnO). With an appropriate Zn^{2+} presence in ZnO-TiO_2 nanocomposites, the specific surface area, total pore volume, charge transfer, and photocatalytic activity were significantly improved. Particularly, the samples containing 30 and 50 wt. % (30ZnO and 50ZnO) showed higher photocatalytic activity towards hydrogen generation, which attributed to higher specific surface areas, larger pore volumes, and lower interface resistance as confirmed by adsorption-desorption isotherms and EIS measurements, respectively. Hence, ZnO-TiO_2 composites with higher than 50 wt. % ZnO were found to be not favorable to attain reasonable photocatalytic activity toward hydrogen generation as specific surface area and pore volume were drastically decreased. © *2013 AIP Publishing LLC*. [http://dx.doi.org/10.1063/1.4808263]

I. INTRODUCTION

Sharp increase in energy costs, scarce natural resources, and the fragility in the global climate have increased the need for renewable, clean energy sources. When considering fuel sources, hydrogen holds a tremendous promise as the ultimate renewable energy resource for

[a)]Author to whom correspondence should be addressed. Electronic mail: rajesh.shende@sdsmt.edu. Tel.: 1 605 394 1231. Fax: 1 605 394 1232.

several reasons. First, the by-product of hydrogen combustion is water, making hydrogen a clean source of energy. In addition, the reaction of hydrogen and carbon dioxide yields hydrocarbon fuels and other industrial chemicals. Currently, industrial hydrogen production is achieved from non-renewable resources, such as methane and petroleum using steam gas reforming. These processes rely on the use of fossil fuels and there is a need to find a renewable, non-polluting source for the production of hydrogen. Efficient photoactive materials capable of harvesting and converting solar energy into stored chemical energy via solar energy-driven direct water splitting are most compelling. Various systems for solar water splitting include semiconductor nanoparticles as photocatalysts, photoelectrodes, molecular donor-acceptor co-catalyst for hydrogen and oxygen evolution, and photoelectrocatalysts.[1] Processes relying solely on sunlight need continuing research for the optimization of hydrogen production. However, the charge separation and transport properties of single and/or conventional materials may not be sufficient for sustainable and economical energy harvesting.

In the case of using the sunlight in its entirety, however, numerous challenges lie ahead in increasing hydrogen production efficiency. A major drawback in achieving high photocatalytic efficiency is the rapid recombination of charge carriers, which has faster kinetics than surface redox reactions.[2] Therefore, it is important to mitigate the recombination rate to improve the efficiency of photocatalysts. Coupled mesoporous semiconductor materials offer an approach for tailoring the transport property, charge separation ability, and minimizing charge recombination leading to an enhancement in a photocatalyst performance. On the way towards improved photoactivity, coupled ZnO-TiO_2 offers a new perspective. Several studies have been directed to the use of ZnO-TiO_2 composites, but most of them are focused on photocatalytic degradation of organic pollutants in water and air, while only a few investigations[3] can be found in the literature on H_2 generation. In very recent study,[4] composites containing up to 10% ZnO in ZnO-TiO_2 were prepared using sol-gel method without the use of a surfactant and demonstrated improved H_2 generation as compared to TiO_2 using ethanol (50 vol. % ethanol) as sacrificial agent. Jiaguo *et al.*[5] investigated fabrication of Ni-doped mesoporous TiO_2 and its photocatalytic activity for hydrogen evolution in methanol aqueous solution (25 vol. % methanol) showing improved activity towards H_2 generation. However, there are only very few reports on the photocatalytic H_2 production over ZnO coupled TiO_2 photocatalyst up to now. Herein, in the present investigation, we prepared the large spectrum of ZnO-TiO_2 compositions containing ZnO concentrations in the range of 10% to 90% using Pluronic P123 surfactant and studied their effectiveness on H_2 generation from aqueous methanol solution (20 vol. % methanol).

As photocatalytic reaction is solely based on the generation of electron-hole pairs by means of band gap excitation, studies of coupled semiconductor materials are essential in developing our understanding of photoinduced charge transport processes. We hypothesize that enhanced photocatalytic water splitting activity in coupled ZnO-TiO_2 nanocomposites will be realized due to effective charge separation at the heterojunction interface leading to decrease in charge recombination and increase in electron and hole lifetimes to carry a designated photocatalytic reaction. Advantages of coupled semiconductors with slightly staggered conduction band edges will be intrinsically built-in potential gradient at the interface facilitating efficient charge separation and interfacial charge transfer. This will lead to prevention of electron-hole recombination before a desired chemical reaction takes place at the surface of semiconductor nanoparticles.[6]

Mesoporous materials with hierarchical and ordered structures are promising candidates for numerous applications such as photocatalysis, dye sensitized solar cells, sensors, etc. Among the semiconductor materials investigated, TiO_2 is the most commonly used semiconductor in solar energy conversion schemes due to its high photosensitivity, non-toxicity, ease of availability, environmentally benign, and low cost. In addition to TiO_2, ZnO has shown some promise for the above mentioned applications.[7] It has comparable bandgap as TiO_2 and a slightly negative conduction band potential and, in principle, will have higher redox potential generating higher photovoltages.[8,9] Furthermore, ZnO is direct bandgap semiconductor and has high exciton binding energy and higher electron mobility than TiO_2.[10] Until now, however, photocatalysis based on ZnO is limited by photocorrosion upon irradiation. On the other hand, TiO_2 has been widely investigated in photocatalysis; however, its efficiency in solar light driven

processes is substantially limited due to wide band gap and charge carrier recombination.[11,12] As such, considerable effort has been devoted to using transition metal and non-metal doping strategies to induce visible light response in UV active photocatalysts such as TiO_2 and ZnO. The effort of modifying the intrinsic band gap of UV absorbing photocatalysts to absorb additional visible light, however, does not necessarily result in visible light response and can even deteriorate the UV photoactivity.[13,14] For instance, the photocatalytic H_2 generation has not been achieved with Cr-doped TiO_2 for water splitting reaction in spite of the fact that such doped TiO_2 shows visible light absorption.[15]

The aim of this work is to synthesize different ZnO-TiO_2 nanocomposites and investigate their photocatalytic performance towards H_2 generation. The photocatalysts were prepared using structure directing surfactant assisted sol-gel method, characterized using various analytical techniques and utilized for hydrogen generation from methanol aqueous media in a semi-batch reactor system. The photocatalytic performance of coupled ZnO-TiO_2 nanocomposites was compared with individual ZnO and commercial TiO_2 P25 photocatalyst nanoparticles.

II. EXPERIMENTAL

A. Materials

All reagents were analytical grade and used as received. Zinc nitrate hexahydrate (98%), titanium (IV) n-butoxide (99%), and Pluronic P123 were obtained from Sigma-Aldrich. Absolute ethanol and methanol were obtained from AAPER, and concentrated hydrochloric acid was purchased from Fisher-Scientific. Commercial TiO_2 P25 was obtained from Degussa. Deionized water was used for the sol-gel synthesis.

B. Synthesis of ZnO-TiO_2 nanocomposites

The ZnO-TiO_2 nanocomposites were synthesized by a sol-gel method. In a typical synthesis, 2.7 g of titanium (IV) n-butoxide and 0.3 g of zinc nitrate hexahydrate were separately dissolved in 7 ml absolute ethanol, which were labeled as sol A and sol B, respectively. Sol A contained 15 wt. % Pluronic P123 as surfactant in addition to titanium (IV) n-butoxide. After magnetic stirring for 10 min, 0.3 ml concentrated hydrochloric acid was added to sol A and stirred for 10 more minutes. Sol B was added slowly into sol A under constant stirring. The obtained clear solution mixture was continuously stirred for next 60 min and following this the gel formation was initiated with the addition of deionized water. The sol was left undisturbed at room temperature for a few hours forming a clear gel. As-prepared gel was oven dried at 80 °C for 12 h. The resultant solid was pulverized with pestle and mortar and calcined in air at 500 °C for 5 h with the heating rate of 1 °C/min. The weight percent ratio of ZnO in ZnO-TiO_2 nanocomposites was varied as 10, 30, 50, 70, and 90. As prepared powdered samples were denoted as 10ZnO, 30ZnO, 50ZnO, 70ZnO, 90ZnO, and ZnO. The number in the code represents weight percent of the ZnO in ZnO-TiO_2. Schematic chart outlining the procedure for the ZnO-TiO_2 photocatalyst preparation is shown in Figure 1.

C. Characterization methods

Phase identification of the mixed oxides samples was carried out by X-ray diffraction (XRD) from Rigaku Ultima IV instrument with PDF-2 database. The diffractometer was operated at 40 kV, 44 mA, (1.76 kW). The angle (2θ) in the range of 10° to 80° was scanned at the rate of 0.25°/min for the powder XRD measurements. The UV-visible diffuse reflectance spectra (DRS) were recorded using a Cary 100 Bio UV-visible spectrophotometer with Praying Mantis diffuse reflection accessory (Harrick Scientific). The Brunauer-Emmett-Teller (BET) specific surface area and Barrett-Joyner-Halenda (BJH) pore size distribution plot of the samples were determined using nitrogen adsorption-desorption isotherms obtained at 77 K using a Quantachrome Novawin 2200e instrument. Transmission Electron Microscopy (TEM) images were obtained using a FEI Tecnai G^2 30 field-emission instrument operating at accelerator voltage of 120 kV. The sample for TEM studies was prepared by suspending a few milligrams in

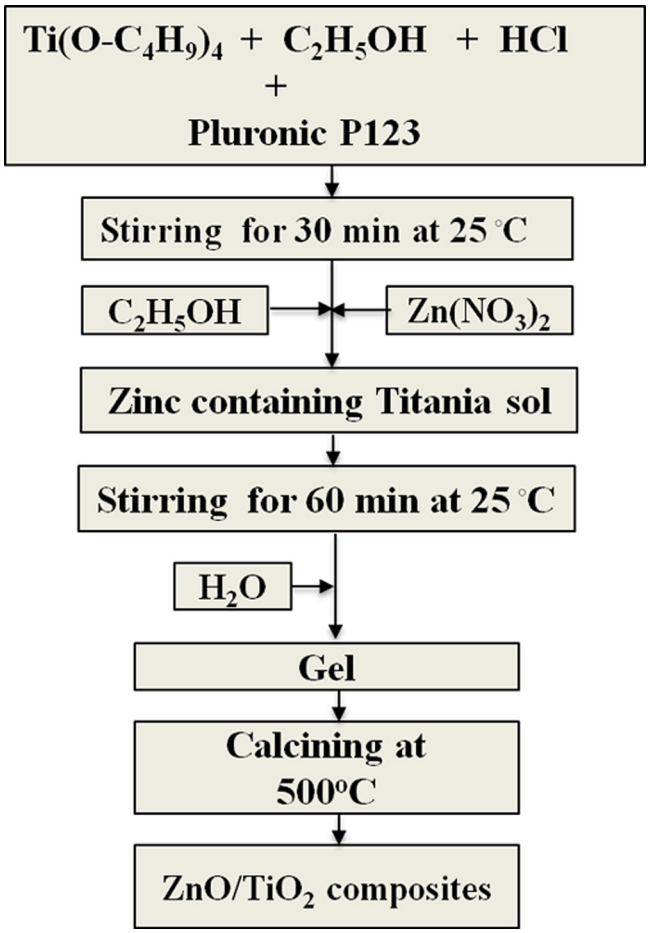

FIG. 1. Schematic flow diagram for the sol-gel synthesis of the ZnO-TiO_2 nanocomposites using a structure directing surfactant template.

ethanol and dispersing the suspension by ultrasonication. A drop of this suspension was placed on a clean copper grid coat containing a carbon film (200 mesh), and allowed to dry overnight in a petri dish prior to collecting images. Raman spectra were taken using a Horiba Jobin Yvon Aramis Raman spectrometer equipped with diode-pumped solid-state (DPSS) and laser of wavelength of 532 nm as light source. Electrochemical impedance spectroscopy (EIS) measurements were made as a function of frequency from 0.05 Hz to 300 kHz using a potentiostat/galvanostat system. The AC voltage amplitude of 10 mV was superimposed on the DC potential and applied to the pellet. The pellet was sandwiched between two stainless steel electrodes and connected to the Gamry-300 system for measuring the impedance at ambient conditions.

D. Photocatalytic reactor setup

The set-up consisted of 5 ml quartz semi-batch reactor provided with UV filter and a light source. The focused intensity and area on the quartz reactor were 0.60 W and 2 cm^2, respectively. A 300 W xenon lamp (Oriel) equipped with an UV-filter ($240 < \lambda < 400$ nm) was employed as the light source.

E. Photocatalytic H_2 evolution

In a typical experiment, 2.0 mg of ZnO-TiO_2 photocatalyst was dispersed in 1.6 ml of H_2O and 0.4 ml methanol (20 vol. %) and placed in a quartz reactor. Prior to irradiation, the suspension of the catalyst was degassed with ultrapure argon for 30 min to completely remove the

dissolved oxygen and to ensure the reactor is in anaerobic conditions. From 3 ml reactor head space, 0.5 ml of product gas was intermittently sampled through the septum and injected into the TCD-equipped SRI 8610C gas chromatograph (GC) with a molecular sieve column at 1, 2, 3, and 4 h time intervals, from which H_2 evolution was measured. A calibration plot was used to quantify the H_2 volume. The photocatalytic H_2 evolution from coupled ZnO-TiO_2 composite was compared with that of P25 as the benchmark.

III. RESULTS AND DISCUSSION

A. Photocatalyst characterization

Mesoporous coupled ZnO-TiO_2 photocatalysts containing different ZnO wt. % (0, 10, 30, 50, 70, 90, and 100) were prepared by the sol-gel method using a structure-directing template as outlined earlier in the experimental section and calcined at 500 °C for 5 h. The powder XRD patterns of the ZnO-TiO_2 composites containing different amounts of ZnO are shown in Figure 2. The XRD pattern reveals peaks that are attributed to different diffraction planes of anatase TiO_2 and consistent with ICDD-PDF-21-1272. At relatively low ZnO loadings (10ZnO and 30ZnO), no diffraction pattern corresponding to ZnO is observed in the composite, suggesting that the ZnO was present as an amorphous phase[16] to produce its characteristic patterns that were also confirmed by TEM and Raman spectral analysis.

In addition, it is possible that at low loadings, some Zn^{2+} ions can substitute in interstitial sites present in TiO_2.[17] With a further increase in Zn^{2+} loadings, several peaks corresponding to the characteristics peaks of pure hexagonal ZnO with a wurtzite structure were observed. XRD data clearly indicate that an increase in the Zn^{2+} content brings about a corresponding increase in the crystallite sizes of ZnO nanoparticles, leading to sharper diffraction peaks. In addition, with increasing ZnO content with respect to TiO_2, the relative diffraction peaks corresponding to

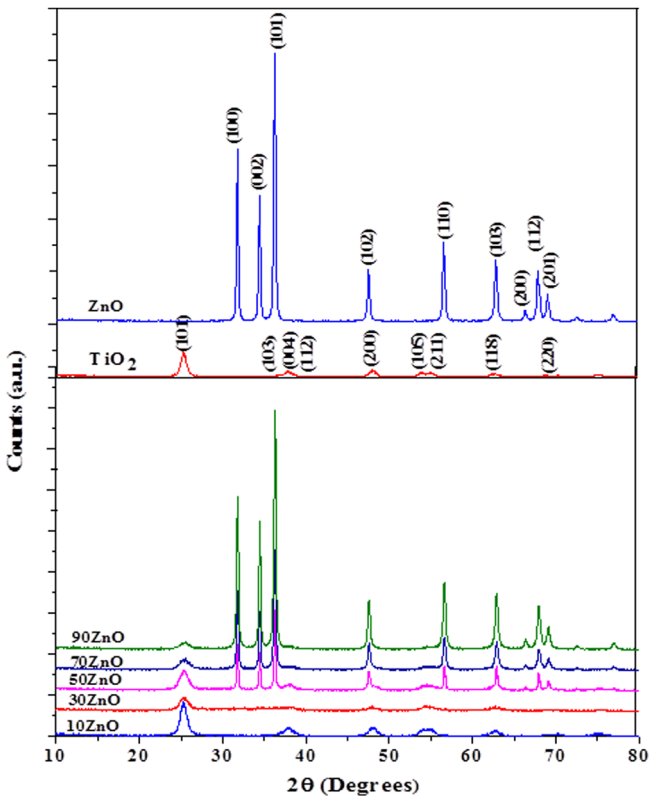

FIG. 2. XRD profiles of ZnO-TiO_2 composites prepared with different Zn^{2+} loading and calcined at 500 °C for 5 h.

anatase gradually weaken and disappear. Furthermore, for the low Zn^{2+} loading, the XRD crystallite sizes of TiO_2 vary from 4.5 to 10 (± 1 nm).

Figures 3(a) and 3(b) show high resolution TEM images of one representative ZnO-TiO_2 composite (50ZnO). These images reveal distinguishable mixed phase grains and well-resolved crystalline plane with *d*-spacing of 0.35 nm corresponding to the presence of (101) plane of anatase and with lattice fringe *d*-spacing of 0.25 nm to the presence of (101) ZnO (Figure 3(b)). The size of over 75 particles was measured from one of the representative TEM images as shown in Figure 3(a). The particles were essentially little aggregated but still appear spherical and ellipsoid in shape individually. The size of these particles was found to be in the range of 6.2 nm to 14.1 nm with the average particle size of 10.04 nm and standard deviation of 1.88 nm.

To derive textural data of ZnO-TiO_2 composites, nitrogen adsorption-desorption isotherms were obtained for calcined samples. Figures 4(a) and 4(b) show the nitrogen adsorption-desorption isotherms and pore size distribution curves, respectively, of pure ZnO as well as coupled ZnO-TiO_2 composites. The isotherm profiles are characterized by the presence of the H2 hysteresis loop typical of a type IV isotherm corresponding to capillary condensation characteristic for mesoporous adsorbents.[18] The hysteresis loops have an upward curvature at a relative pressure above 0.4. This upward curvature indicates the presence of cylindrical mesopores.[15] The shape of the isotherms and steepness seem to be influenced by ZnO content. For 70ZnO sample or higher Zn^{2+} loading, the adsorption and desorption branches were nearly parallel, probably indicating highly uniform pore size distribution. As clearly shown in Figure 4(a), pure ZnO nanoparticles have lowest N_2 volume adsorption indicating lower surface areas. Effects of ZnO loading on the BET specific surface areas, pore volumes, and pore diameters are listed in Table I. Both the surface areas and pore volumes increased systematically with ZnO contents, pass through a maximum, and show volcano shape dependence on ZnO contents. Similar trends were observed after loading or mixing TiO_2 with ZnO or ZrO_2.[19,20] The surface area and pore volume of ZnO-TiO_2 composite reached maximum with the 50 wt. % ZnO loading. It was also found that the specific surface areas of 30ZnO and 50ZnO were significantly higher than Degussa TiO_2 or pure ZnO. Generally, higher surface area material is beneficial for superior photocatalytic activity.

The influence of Zn^{2+} contents on electronic structure of ZnO-TiO_2 nanocomposites was examined by DRS. Figure 5 depicts room temperature UV-visible diffusive reflectance spectra of the ZnO and ZnO-TiO_2 composites. In a semiconductor such as ZnO and TiO_2, light is only absorbed if it has energy that is greater than the energy required to excite an electron from the valence band to the conduction band of the material. ZnO is a direct band gap semiconductor with bandgap energy of 3.3 eV. On the other hand, the TiO_2 is an indirect bandgap

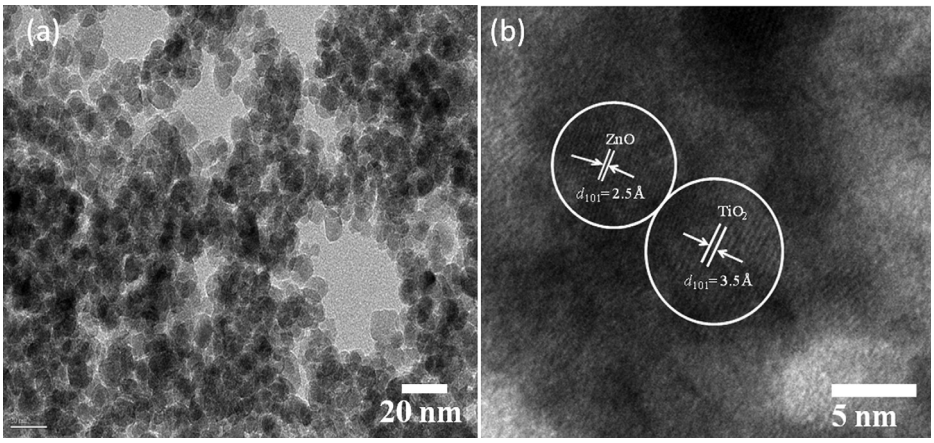

FIG. 3. HRTEM images of 50ZnO composite prepared by the sol-gel method and annealed at 500 °C, confirming a spherical structure with lattice fringes 3.5 Å and 2.5 Å of (101) and (101) planes, respectively, corresponding to TiO_2 and ZnO. The images (a) and (b) show particle size and lattice fringes, respectively. The image (b) is the magnified TEM image of 50ZnO composite showing a close neighborhood contacts between ZnO and TiO_2 nanoparticles.

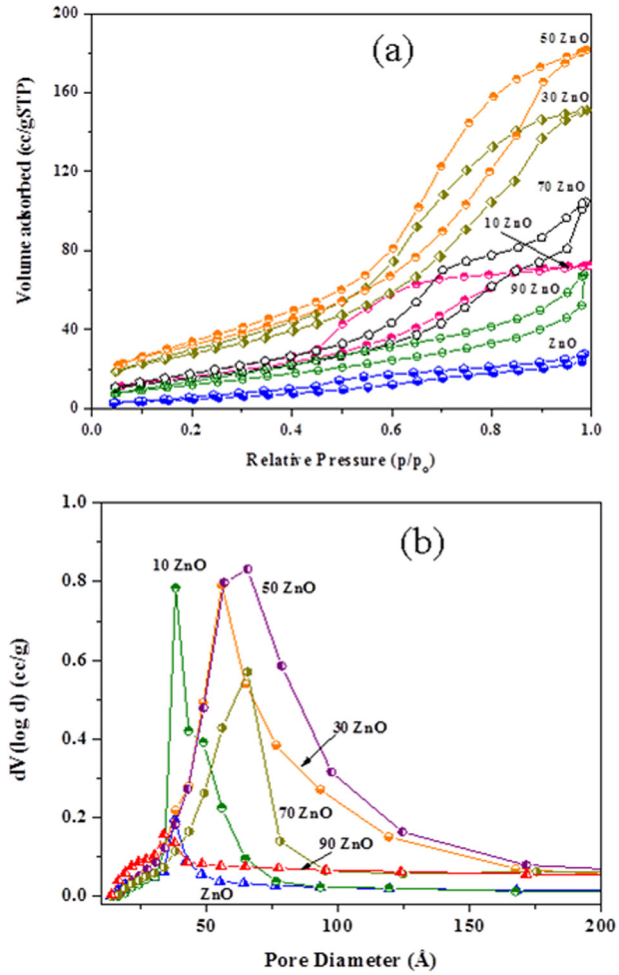

FIG. 4. Nitrogen physisorption isotherms (a) and corresponding pore size distribution (b) of mesoporous ZnO and ZnO-TiO_2 composites prepared by sol-gel method.

semiconductor with bandgap energy of 3.2 eV (387.5 nm) for anatase. The excitonic peaks of ZnO and their composites, exhibit a blue shift in the excitonic peak with respect to their bulk.[21–23] This blue shift in absorption band-edge gives a clear indication to increasing quantum confinement. The presence of different native defect concentration density on the surface of coupled ZnO-TiO_2 nanocomposites is also expected to contribute to spectral shifts.[24,25] The

TABLE I. Photocatalytic activities of ZnO-TiO_2 nanocomposites for H_2 production from an aqueous methanol solution.

	Crystallite size (nm)					
Reference	ZnO	TiO_2	Surface area (m^2/g)	Pore volume (cm^3/g)	E_g (eV)	H_2 evolution (ml/g)
TiO_2 P25	…	…	50	…	…	8.01
10ZnO	…	7.9	64	0.112	3.31	6.06
30ZnO	…	4.6	107	0.233	3.35	17.3
50ZnO	5.0	…	122	0.280	3.37	16.6
70ZnO	4.0	…	59	0.169	3.25	0.98
90ZnO	3.8	…	48	0.105	3.26	0.91
ZnO	3.6	…	19	0.048	3.37	0.00

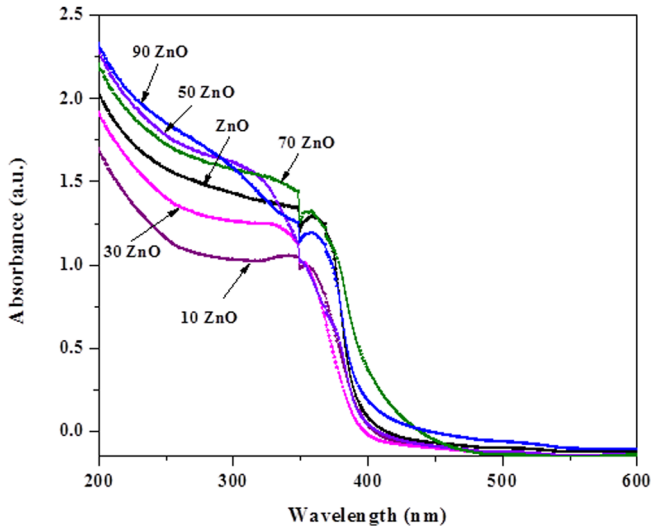

FIG. 5. UV-visible DRS of ZnO-TiO_2 composites and ZnO, which were calcined at 500 °C for 5 h.

quantum confinement can be observed in Table I with increasing energy band gaps, giving rise to a blue shift of the band edges as the crystal size decreases.

The plot of modified Kubelka-Munk function versus energy $((\alpha h\nu)^2$ as a function of $h\nu)$ for indirect bandgap of ZnO-TiO_2 nanocomposites was analyzed. From this plot (not included), the optical bandgap was obtained by extrapolating a corresponding linear region on the plots intersecting energy axis. The estimated bandgap energies are given in Table I. For all analyzed samples, the spectra showed UV absorbance edges between 368 and 395 nm (~3.2–3.37 eV), which corresponds to the bandgap energy of bulk individual TiO_2 and ZnO. It was found that the optical bandgap for the composites slightly increased with increase in ZnO loadings up to 50ZnO and thereafter decreased. It is noted that the absorption edge corresponding to the ZnO-TiO_2 composites shifted to shorter wavelengths (i.e., larger bandgaps) upon increased ZnO contents up to 50 wt. % with respect to known phase pure TiO_2. Therefore, the optical band gap is the function of Zn^{2+} loading and there is an increase with increasing ZnO loading.

Raman spectroscopic studies were also carried out and the results are presented in Figure 6. We tried to compare the effect of Zn^{2+} loading, on the presence of acoustic modes, and on the dynamics of non-polar (E2) surface optical phonon modes in ZnO-TiO_2 nanocomposites. The

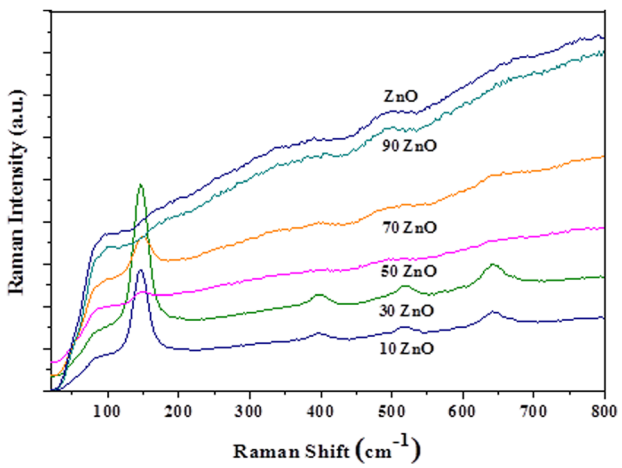

FIG. 6. Raman spectra of all samples prepared in this study.

positions and intensity of Raman modes at 146.5, 396.7, 519.2, and 640 cm^{-1} corresponded well with anatase phase of TiO_2 as reported by others[26–28] and it is typical for TiO_2 samples annealed at 500 °C under oxygen atmosphere. The spectra of the anatase TiO_2 phase confirm the phase obtained from the XRD analysis. Upon decreasing the weight percent of TiO_2, the intensity of these vibrational bands rapidly decreases as depicted in Figure 6. Weak and broadened peaks centered around 490 cm^{-1}, attributed to a surface optical phonon of ZnO could be seen in samples with relatively higher ZnO amounts. Relatively weak signal of the vibrational mode might suggest poor crystallinity of the ZnO nanostructures in the composite. Similar trends were observed with peak intensities that drastically reduced after the addition of ZnO along with those of other spectral modes.[29] It is worth noting that with high Zn^{2+} contents, the vibrational modes of TiO_2 in the composites were weakened.[30]

To obtain insight into the improvements in charge carrier and generation due to suitable heterojunction interface formation in ZnO-TiO_2 composites, EIS measurements were carried out over the frequency range of 0.05 Hz–300 kHz. EIS analysis revealed appreciable difference in the charge transfer resistance in commercial TiO_2 P25, ZnO, and coupled ZnO-TiO_2 composites. Figure 7 depicts the EIS Nyquist plots of nominally phase pure commercial TiO_2 P25, ZnO materials, and the most active coupled ZnO-TiO_2 composites. Typically in higher frequency region, the AC impedance spectral response exhibits a semicircle and sloping line in the low-frequency region. It has been widely recognized that the semicircle can be attributed to the charge transfer resistance through heterojunction interface. The sloping line in the low-frequency region probably represents the Warburg impedance, which is related to semi-infinite diffusion of the charge carriers.[31] It is obvious that the charge transfer resistance to the electron transfer decreased appreciably with the introduction of ZnO in comparison with commercial TiO_2 P25. This suggests that the coupling of ZnO with TiO_2 could effectively improve charge transport by providing direct conduction pathways to ZnO-TiO_2 composites while maintaining high surface area leading to high photocatalytic activity towards H_2 generation. This is an indirect indication that nanocomposites containing a heterojunction interface are more efficient than their single-phase counterparts. The improved photocatalytic activity is attributed to effective electron/hole separation due to the presence of suitable heterojunction, which reduces charge carrier recombination and increases electron and hole lifetimes for desired photocatalytic reactions.

B. Photocatalytic H_2 generation from aqueous methanol solution

The photocatalytic hydrogen evolution over commercial TiO_2 P25 nanoparticles, ZnO nanoparticles, and coupled ZnO-TiO_2 nanocomposites was investigated in an aqueous media in

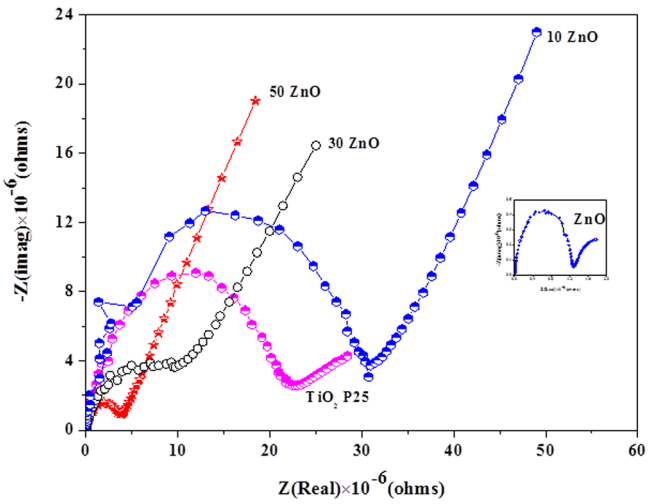

FIG. 7. Nyquist plots of commercial TiO_2 P25, and ZnO, 10ZnO, 30ZnO, and 50ZnO nanocomposites, which were annealed for 5 h at 500 °C. The frequency range was 300 kHz-50 mHz with amplitude of 10 mV.

the presence of methanol as electron donor under UV-light irradiation. The presence of an electron donor other than water is crucial for photocatalytic H_2 production, since little H_2 is produced without added electron donors even under UV light irradiation. In this setup, methanol functions primarily as hole traps to prevent rapid electron-hole recombination.[32] The H_2 generation efficiency over commercial TiO_2 P25 from aqueous methanol media is much lower than that of 30ZnO and 50ZnO nanocomposites, which is mainly due to the fast charge recombination and backward reaction (thermodynamically favourable reaction of hydrogen with oxygen to form water). As depicted in Figure 7, the presence of the ZnO-TiO_2 heterojunction interface is desirable as it can reduce the solid-liquid charge-transfer resistance leading to reduced effective recombination rate. Under illumination, ZnO-TiO_2 was characterized by a faster charge carrier transfer as denoted by the lower solid-liquid charge transfer resistance and higher electron migration. The improved H_2 generation obtained for 30ZnO and 50ZnO as compared with commercial TiO_2 P25 or ZnO may be also explained by the decreased rate of electron–hole recombination across the nanocomposite-liquid interface due to the presence of structurally and electronically favorable heterojunction.

Figure 8 shows effects of ZnO loading on the rates of hydrogen evolutions. All ZnO-TiO_2 nanocomposites exhibited significant photocatalytic activities towards H_2 evolution. However, the relative hydrogen yield over ZnO-TiO_2 composites varies with the percent composition of ZnO to TiO_2. The enhanced photocatalytic activity in 30ZnO composite can be explained in terms of the injection of conduction band electrons from ZnO into the lower-lying bands of the TiO_2 material. The 50ZnO photocatalyst shows high H_2 evolution rate during initial reaction time period, but longer irradiance resulted in a decrease of H_2 evolution rate with respect to 30ZnO. The higher initial rate of hydrogen generation associated with 50ZnO is more likely due to its higher surface area, pore volume, and slightly depressed high-frequency semicircle as seen in Figure 7 indicating that low resistance to charge transfer among other composites in comparison with 30ZnO. However, decreased hydrogen evolution rate can be speculated to be related to photocorrosion of 50ZnO under longer UV-light illumination. Upon UV light irradiation, photocorrosion with ZnO assisted photocatalysis is widely known as a major issue.[33] Our experimental results demonstrate that excessive Zn^{2+} above the optimal loading would result in a sharp decrease in photocatalytic activity. ZnO alone showed no measureable H_2 evolution,

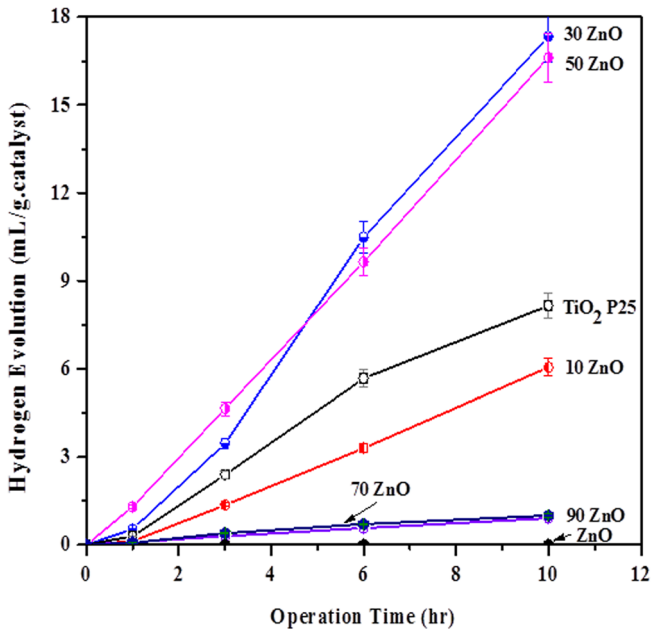

FIG. 8. Photocatalytic H_2 evolution from water-methanol media in the presence of coupled ZnO-TiO_2 composites relative to commercial TiO_2 P25 and pure phase ZnO.

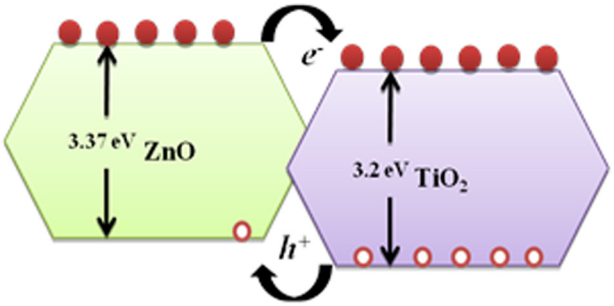

FIG. 9. Schematic representation showing electron/hole separation process at coupled ZnO-TiO_2 heterojunction interface.

which might be due to low specific surface area and photocorrosion induced self-oxidation that leads to rapid photocatalyst inactivation.[34]

The enhancement in photocatalytic activity in ZnO-TiO_2 composite mainly attributed to the formation of favorable active reaction sites by effective interfacial contacts between ZnO and TiO_2 components, which appears to be crucial for the charge transfer.[35] As listed in Table I, the improvement in photocatalytic hydrogen evolution can be attributed to several other factors such as specific surface area and total pore volume of ZnO-TiO_2 composites as it was significantly increased with respect to either ZnO or TiO_2 P25 alone. The specific surface area increased with increasing the amount of Zn^{2+} content in the composite, reaching a maximum at 50% weight loading and diminishes with further increase in Zn^{2+} loading. The highest value in specific surface area obtained for 30 and 50 wt. % Zn^{2+} loadings was determined to be $106\,m^2\,g^{-1}$ and $122\,m^2\,g^{-1}$, respectively, and as compared to that of commercial TiO_2 P25 ($50\,m^2\,g^{-1}$). The improvement in photocatalytic activity may be ascribed to the larger surface area (as more reactive surface sites are available) and the presence of high porosity, i.e., large pore size distribution that favors efficient diffusion or molecule trafficking.

ZnO and TiO_2 are both semiconductor photocatalysts that can only be activated by UV light. Shown in Figure 9 is the tentatively proposed charge and energy distribution diagram to explain the presence ZnO-TiO_2 heterojunction based on observations from TEM images and EIS analysis. Moreover, ZnO has known to have the onset flat band potential more negative that of TiO_2.[36,37] The Fermi level or quasi-Fermi level is a collective property of the carriers and is strongly influenced by the disorder in the material as well as by the presence of heterostructures.[38,39] Light incident on the surface of ZnO-TiO_2 induces a charge separation between excited electron and its valance band hole, where electrons transfer from the ZnO conduction band to the TiO_2 conduction band and conversely, holes transfer from the TiO_2 valence band to the ZnO valence band. The presence of ZnO-TiO_2 heterojunction as the potential barrier may limit the likelihood of electron/hole recombination. This increases the availability of the electrons or holes to migrate to the TiO_2 or ZnO surface of the ZnO-TiO_2 composite photocatalysts and consequently improves the occurrence of redox processes.

In order to illustrate the photocatalytic hydrogen formation from an aqueous methanol solution using ZnO-TiO_2 composites, possible reaction pathways are suggested below

$$ZnO/TiO_{2(s)} + CH_3OH/H_2O_{(l)} \overset{h\nu}{\leftrightarrow} H_2CO + H_{2\,(g)}, \tag{1}$$

$$ZnO/TiO_{2(s)} + H_2CO/H_2O_{(l)} \overset{h\nu}{\leftrightarrow} H_2CO_2 + H_{2\,(g)}, \tag{2}$$

$$ZnO/TiO_{2(s)} + H_2CO_2/H_2O_{(l)} \overset{h\nu}{\leftrightarrow} CO_2 + H_{2\,(g)}. \tag{3}$$

The oxidation of methanol produces formaldehyde (H_2CO) and hydrogen suggesting that CH_3O is an active intermediate leading to H_2CO.[40,41] The product, formaldehyde (HCHO), could be further oxidized to methanoic acid (H_2CO_2). However, no subsequent H_2CO_2 photooxidation has taken place as no CO_2 formation was observed from GC analysis due to partial

oxidation of methanol. According to reaction 3, the generated CO_2 in the suspension should result in the elevation of the acidity of suspension. Nevertheless, from pH measured (pH $\approx$ 5.5) before and after 10 h of irradiation reaction process, the pH remained the same confirming partial oxidation of methanol. Separate experiments confirmed the presence of formaldehyde under our experimental conditions.

Dispersed photocatalyst powder in a photochemical reactor for water splitting is not suitable for practical and sustainable hydrogen production. In photochemical reaction setup, during water oxidation and reduction, molecular hydrogen and oxygen are generated simultaneously and recombines again on catalyst surface forming water (thermodynamically favourable reaction). To overcome this challenge, the reactor may be designed with suitable nanomachinery (e.g., nanobeakers) to perform water oxidation and reduction separately that will effectively eliminate the backward recombination reaction. Self-supported transparent photocatalyst nanobeakers capable of oxidation and reduction at two ends may be essential for hydrogen production. The designing and engineering of the nanobeakers are in progress in our laboratory.

IV. CONCLUSIONS

In this study, we synthesized and characterized noble-metal-free mesoporous coupled ZnO-TiO_2 photocatalyst nanocomposites with various compositions. These photocatalysts were investigated for photocatalytic H_2 generation from aqueous methanol solution. The coupled ZnO-TiO_2 photocatalysts with 30ZnO and 50ZnO have shown enhanced H_2 production compared to individual ZnO or commercial TiO_2 P25. The hydrogen evolution and performance of photocatalyst increased with the moderate increase in Zn^{2+} content, indicating that coupling had a positive synergic effect on improving photocatalytic activity in ZnO-TiO_2 composites. With an appropriate Zn^{2+} loading, the specific surface and total pore volume increased, consequently resulting in a large number of reaction sites on the composites leading to enhanced photocatalytic activity. Among the photocatalyst nanocomposites investigated, the 30ZnO photocatalyst exhibited higher H_2 generation over a time period of 10 h and its H_2 generation capability was found to be highest among other photocatalyst materials. The improved photocatalytic activity toward H_2 generation was mainly attributed to high surface area, large pore volume, and lower interface charge resistance leading to effective electron-hole separation at the heterojunction between ZnO and TiO_2 phases. This allowed additional transfer of charges from ZnO to TiO_2 and reduced the charge recombination thereby increasing the electron and hole lifetimes. The depressed semicircle in high-frequency region shown by EIS measurements due to Zn^{2+} loading is, therefore, an indicative of the influence of ZnO on the conductivity and charge mobility of TiO_2.

ACKNOWLEDGMENTS

The authors acknowledge the financial and research assistantship support from NSF-DGE-0903685. NSF-EPS-0903804, DE-EE0000270, NSF-CHE-0722632, and NSF-CHE-0840507 are also acknowledged. We are also thankful to N. Netzer and Professor C. Jiang for assistance with Raman and Dr. C. Lin with TEM studies.

[1]W. J. Youngblood, S.-H. A. Lee, K. Maeda, and T. E. Mallouk, Acc. Chem. Res. **42**, 1966 (2009).
[2]M. Zhang, T. An, X. Liu, X. Hu, G. Sheng, and J. Fu, Mater. Lett. **64**, 1883 (2010).
[3]C. M. Janet, S. Navaladian, B. Viswanathan, T. K. Varadarajan, and R. P. Viswanath, J. Phys. Chem. C **114**, 2622 (2010).
[4]A. Pérez-Larios, R. Lopez, A. Hernández-Gordillo, F. Tzompantzi, R. Gómez, and L. M. Torres-Guerra, Fuel **100**, 139 (2012).
[5]J. Yu, Y. Hai, and B. Cheng, J. Phys. Chem. C **115**, 4953 (2011).
[6]A. Fujishima, T. N. Rao, and D. A. Tryk, J. Photochem. Photobiol. C **1**, 1 (2000).
[7]D. Schlettwein, T. Oekermann, T. Yoshida, M. Tochimoto, and H. Minoura, J. Electroanal. Chem. **481**, 42 (2000).
[8]K.-S. Ahn, Y. Yan, S. Shet, K. Jones, T. Deutsch, J. Turner, and M. Al-Jassim, Appl. Phys. Lett. **93**, 163117 (2008).
[9]P. Kajitvichyanukul and T. Sungkaratana, Asian J. Energy Environ. **7**, 258 (2006).
[10]A. S. Huss, J. E. Rossini, D. J. Ceckanowicz, J. N. Bohnsack, K. R. Mann, W. L. Gladfelter, and D. A. Blank, J. Phys. Chem. C **115**, 2 (2011).
[11]M. Ni, M. K. H. Leung, D. Y. C. Leung, and K. Sumathy, Renewable Sustainable Energy Rev. **11**, 401 (2007).
[12]T. K. Tseng, Y. S. Lin, Y. J. Chen, and H. Chu, Int. J. Mol. Sci. **11**, 2336 (2010).

[13]H. Irie, Y. Watanabe, and K. Hashimoto, J. Phys. Chem. B **107**, 5483 (2003).
[14]G. Liu, C. Sun, L. Cheng, Y. Jin, H. Lu, L. Wang, S. C. Smith, G. Q. Lu, and H.-M. Cheng, J. Phys. Chem. C **113**, 12317 (2009).
[15]T. Ikeda, T. Nomoto, K. Eda, Y. Mizutani, H. Kato, A. Kudo, and H. Onishi, J. Phys. Chem. C **112**, 1167 (2008).
[16]Y. V. Kolen'ko, K. A. Kovnir, A. I. Gavrilov, A. V. Garshev, P. E. Meskin, B. R. Churagulov, M. Bouchard, C. Colbeau-Justin, O. I. Lebedev, G. Van Tendeloo, and M. Yoshimura, J. Phys. Chem. B **109**, 20303 (2005).
[17]X. Yuan, X. Shi, M. Shen, W. Wang, L. Fang, F. Zheng, and X. Wu, J. Alloys Compd. **485**, 831 (2009).
[18]J. B. Condon, *Surface Area and Porosity Determinations by Physisorption: Measurements and Theory* (Elsevier, Amsterdam, 2006).
[19]F. Li, Y. Wang, W. Xue, and X. Zhao, J. Chem. Technol. Biotechnol. **84**, 48 (2009).
[20]B. Neppolian, Q. Wang, H. Yamashita, and H. Choi, Appl. Catal., A **333**, 264 (2007).
[21]Z. Fan and J. G. Lu, J. Nanosci. Nanotechnol. **5**, 1561 (2005).
[22]K.-F. Lin, H.-M. Cheng, H.-C. Hsu, L.-J. Lin, and W.-F. Hsieh, Chem. Phys. Lett. **409**, 208 (2005).
[23]O. Taratula, E. Galoppini, D. Wang, D. Chu, Z. Zhang, H. Chen, G. Saraf, and Y. Lu, J. Phys. Chem. B **110**, 6506 (2006).
[24]A. B. Djurišić and Y. H. Leung, Small **2**, 944 (2006).
[25]G. Patwari and P. Kalita, Nanosci. Nanotechnol.: Int. J. **2**, 13 (2012).
[26]L. Miao, S. Tanemura, S. Toh, K. Kaneko, and M. Tanemura, J. Cryst. Growth **264**, 246 (2004).
[27]Y. Lei, L. D. Zhang, and J. C. Fan, Chem. Phys. Lett. **338**, 231 (2001).
[28]D. Bersani, P. P. Lottici, and X.-Z. Ding, Appl. Phys. Lett. **72**, 73 (1998).
[29]K. Mallick and M. S. Scurrell, Appl. Catal., A **253**, 527 (2003).
[30]S. Tao and J. T. S. Irvine, J. Solid State Chem. **165**, 12 (2002).
[31]B. Neppolian, H. C. Choi, S. Sakthivel, B. Arabindoo, and V. Murugesan, J. Hazard. Mater. **89**, 303 (2002).
[32]C.-H. Liao, C.-W. Huang, and J. Wu, Catalysts **2**, 490 (2012).
[33]K. Maeda and K. Domen, in *Photocatalysis*, edited by C. A. Bignozzi (Springer, Berlin, 2011), Vol. 303, p. 95.
[34]T.-y. Peng, H.-j. Lv, P. Zeng, and X.-h. Zhang, Chin. J. Chem. Phys. **24**, 464 (2011).
[35]L. Li, G. S. Rohrer, and P. A. Salvador, J. Am. Ceram. Soc. **95**, 1414 (2012).
[36]J. Bisquert and G. Garcia-Belmonte, J. Phys. Chem. Lett. **2**, 1950 (2011).
[37]M. Shen and M. A. Henderson, J. Phys. Chem. Lett. **2**, 2707 (2011).
[38]Q. Guo, C. Xu, Z. Ren, W. Yang, Z. Ma, D. Dai, H. Fan, T. K. Minton, and X. Yang, J. Am. Chem. Soc. **134**, 13366 (2012).
[39]G. Garcia-Belmonte and J. Bisquert, Appl. Phys. Lett. **96**, 113301 (2010).
[40]R. Gao, J. Stark, D. W. Bahnemann, and J. Rabani, J. Photochem. Photobiol., A **148**, 387 (2002).
[41]C. Zhou, Z. Ma, Z. Ren, X. Mao, D. Dai, and X. Yang, Chem. Sci. **2**, 1980 (2011).